

# Rain-wind induced vibration of inclined stay cables. Part II: Mechanical modeling and parameter characterisation

Nicola Cosentino<sup>†</sup>

*DISTART, University of Bologna, Via Risorgimento 2, 40136 Bologna, Italy*

Olivier Flamand<sup>‡</sup>

*Centre Scientifique et Technique du Bâtiment, 11 rue Henri Picherit, 44000 Nantes, France*

Claudio Ceccoli<sup>‡†</sup>

*DISTART, University of Bologna, Via Risorgimento 2, 40136 Bologna, Italy*

*(Received September 9, 2002, Accepted November 17, 2003)*

**Abstract.** This paper presents a mechanical model of Rain-Wind Induced Vibration (RWIV) of stay cables. It is based on the physical interpretation of the phenomenon as given in Cosentino, *et al.* (2003, referred as Part I). The model takes into account all the main forces acting on cable, on the upper water rivulet (responsible of the excitation) and the cable-rivulet interaction. It is a simplified (cable cross-sectional and deterministic) representation of the actual (stochastic and three-dimensional) phenomenon. The cable is represented by its cross section and it is subjected to mechanical and aerodynamic (considering the rivulet influence) forces. The rivulet is supposed to oscillate along the cable circumference and it is subjected to inertial and gravity forces, pressure gradients and air-water-cable frictions. The model parameters are calibrated by fitting with experimental results. In order to validate the proposed model and its physical basis, different conditions (wind speed and direction, cable frequency, etc.) have been numerically investigated. The results, which are in very good agreement with the RWIV field observations, confirm the validity of the method and its engineering applicability (to evaluate the RWIV sensitivity of new stays or to retrofit the existing ones). Nevertheless, the practical use of the model probably requires a more accurate calibration of some parameters through new and specifically oriented wind tunnel tests.

**Keywords:** wind induced vibrations; rain; cable dynamics; water rivulet; bridges.

---

## 1. Introduction

In Part I, the Rain Wind Induced Vibration (RWIV) mechanism has been discussed and a physical interpretation has been given. Different numerical models have been proposed in literature

---

<sup>†</sup> Research Fellow

<sup>‡</sup> Research Engineer

<sup>‡†</sup> Professor

(Yamaguchi 1990, Zasso, *et al.* 1992, Ruscheweyh 1999, Geurst, *et al.* 1998) to simulate RWIVs, basically based on a galloping type instability. Other interpretative models (Matsumoto 2000, Verwiebe and Ruscheweyh 1998) are presented only from a qualitative point of view. Anyway, none of the existing numerical or interpretative models are able to accurately describe the RWIV features (such as the limited wind speed, yaw angle, etc). In addition, none of these models takes into account the influence of the Reynolds number ( $Re$ ) on the exciting mechanism, even if the correlation between  $Re$  and the RWIV occurrence has been pointed out since the firsts full scale observations (Matsumoto, *et al.* 1989).

The exciting mechanism (as explained in Part I) is really complex and hard to describe with a complete model. A statistical model should be the only possibility to take into account all the parameters involved in the rivulet motion, its unsteady dimensions, the influence of the rivulet on the air flow and, thus, on the aerodynamic forces responsible of the excitation. Unfortunately, even if a wide experimental campaign has been carried out, the recorded data are not sufficient to calibrate a stochastic model (in fact, experiments were carried out before the exciting mechanism was pointed out and, hence, they were not specifically oriented to the calibration of a specific mechanical model parameters). Nevertheless, the obtained data have definitely evidenced different interesting aspects for the comprehension of the RWIV mechanism (Part I) and they can be the starting point for future specific investigations.

In this paper, a deterministic mechanical model is proposed. It is based on a two-dimensional description of the cable cross section, without taking into account cable-axial aspects as, for instance, the longitudinal correlation of the exciting forces. Therefore the model is not able to foresee the excited modes and their precise amplitude. The upper water rivulet, responsible of the excitation, is modelled as a secondary oscillator, moving on the cable circumference. Thus, the global model is a 3 DOF system. The excitation is determined by the rivulet-cable movements interaction.

The main purpose of the proposed model is to validate the explanation of the exciting mechanism (Part I) and to evaluate the influence of the different parameters and their order of magnitude. Of course, further investigations will be necessary to improve the accuracy of the model (and, possibly, to formulate a stochastic and 3D one) and to allow a reliable engineering use of the model itself.

## 2. Mechanical model and constitutive equations

The schemes of the forces acting on the cable and on the rivulet are shown in Figs. 1 and 2. Due to the yaw ( $\beta$ ) and inclination ( $\alpha$ ) angles, the wind “sees” the cable under the incidence angle ( $\gamma$ ) derived as:

$$\gamma = 90^\circ - \arccos\left(\frac{\sin\alpha \cdot \sin\beta}{\sqrt{\sin^2\alpha + \cos^2\alpha \cdot \cos^2\beta}}\right) \quad (1)$$

Furthermore,  $\beta^* = \arcsin(\cos\alpha \sin\beta)$  is the effective yaw angle between the cable axis and the wind. Thus, the wind speed component orthogonal to the cable axis is:  $U_r = U_0 \cos\beta^*$ .

Due to the cable movement, the unsteady apparent wind speed and the relative incidence angle are respectively  $\mathbf{U} = \mathbf{U}_r - \dot{\mathbf{X}}$  and  $\gamma - \delta\gamma$ ,  $\mathbf{X} = (X_1, X_2)$  being the instantaneous cable position with respect to the static equilibrium position and  $\delta\gamma$  the angle between vectors  $\mathbf{U}_r$  and  $\mathbf{U}$  (positive if  $\mathbf{U}$  is clockwise rotated from  $\mathbf{U}_r$ ).

The cable is subjected to inertial forces, structural stiffness, structural damping and aerodynamic forces. The latter can be expressed as the sum of drag forces (assumed to be quasi-steady and acting

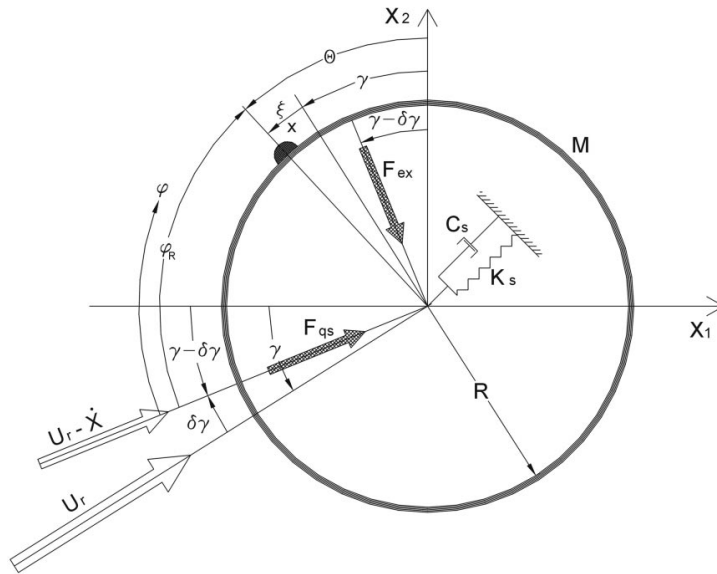


Fig. 1 Scheme of cross-sectional cable model with the upper rivulet

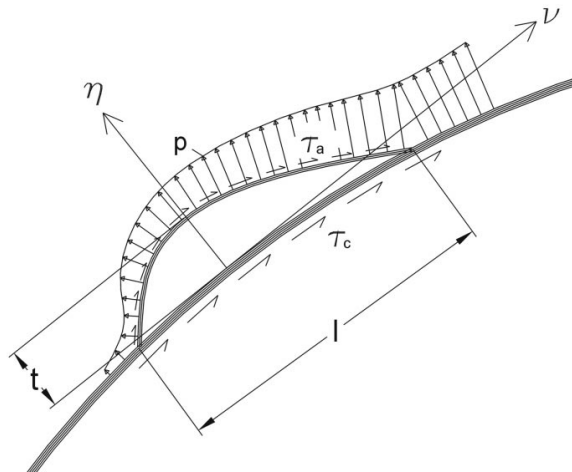


Fig. 2 Scheme of the rivulet and its loads

along the instantaneous in-wind direction,  $\mathbf{F}_{qs} = 1/2 \rho_a DC_D \mathbf{U} |U|$ ) and aeroelastic excitation determined by the presence of the rivulet ( $\mathbf{F}_{ex}$ —acting along the instantaneous cross-wind direction, as observed in Part I). Due to the small weight of the water film, the rivulet mass-forces on the cable can be neglected. Thus,

$$\mathbf{M}\ddot{\mathbf{X}} + \mathbf{C}_s\dot{\mathbf{X}} + \mathbf{K}_s\mathbf{X} = \frac{1}{2}\rho_a DC_D \mathbf{U} |U| + \mathbf{F}_{ex} \quad (2)$$

represents the dynamic equilibrium equation of the cable unit length.  $\mathbf{M}$ ,  $\mathbf{C}_s$ ,  $\mathbf{K}_s$  and  $\mathbf{X}$  are the cable mass, structural damping, stiffness matrices and position vector respectively. They are referred to

the unit length, taking into account the excited (observed or hypothesized) mode features. Of course, in this simplified two-dimensional model, the excitation is supposed to be single-mode. Such a simplification is not too far from the actual behaviour of RWIVs, as observed in different full scale measurements (Main, *et al.* 2001). In Eq. (2),  $\mathbf{U} = \mathbf{U}_r - \dot{\mathbf{X}}$  is the instantaneous normal to the cable wind speed and  $U$  is its magnitude,  $D$  is the cable diameter,  $C_D$  is the drag coefficient,  $\rho_a$  is the air density.  $\mathbf{F}_{ex}$  will be explained below.

As it is shown in Fig. 2, the rivulet is subjected to the following forces: the external pressure gradients, determined by variable pressure  $p$ ; the air-water friction  $\tau_a$ ; the cable-water friction  $\tau_c$  (or rivulet-base carpet friction - see Part I); the gravity effects due to gravity  $g$  and support (cable) acceleration; the inertial effects due to the rivulet acceleration itself. Due to the presence of the base carpet (Part I), the rivulet-cable surface tension can be neglected.

Pressure gradients (as well as all other surface forces) are assumed to be constant within the instantaneous rivulet width  $l$ . The rivulet surface is defined by a function  $\eta = \eta(v)$  (Fig. 2). Generally, both the rivulet dimensions and its thickness-width ratio can change (Part I) but in this simplified model they are assumed to be constant and equal to their mean values derived from wind tunnel measurements (Part I). Nevertheless, the effect of rivulet dimension variations on air-water interaction will be indirectly taken into account by mean of the rivulet velocity (which influences the rivulet dimensions as shown in Part I). In such hypothesis, simple analytical developments (Cosentino 2002) show that the rivulet dynamic equilibrium can be expressed as:

$$\begin{aligned} & \rho_w \cdot l \cdot t \cdot \psi_v (-\ddot{x} + \ddot{X}_1 \cos \theta + \ddot{X}_2 \sin \theta + g \cdot \cos \alpha \sin \theta) + \\ & + \frac{1}{2} \cdot \left. \frac{\partial C_p}{\partial \varphi} \right|_{\varphi = \varphi_R} \cdot \rho_a \cdot U^2 \cdot \frac{1}{R} \cdot l \cdot t \cdot \psi_v - \frac{1}{2} \cdot \rho_a \cdot U^2 \cdot f_a(\varphi_R) \cdot l - \dot{x} \cdot f_c \cdot l = 0 \end{aligned} \quad (3)$$

where  $l$ ,  $t$ ,  $\xi$ ,  $X_1$ ,  $X_2$ ,  $\theta$  and  $x = \xi \times R$  are defined in Figs. 1 and 2;  $\varphi$  is the angular location along the cylinder at which the pressure is monitored (clockwise from the instantaneous stagnation point);  $\varphi_R = \pi/2 - \xi - \delta\gamma$  is the actual position of the rivulet,  $\rho_w$  is the water density;  $\psi_v$  is a rivulet shape factor (such that the rivulet cross area results  $l \times t \times \psi_v$ );  $R$  is the cable external radius;  $C_p$  is the local pressure coefficient;  $f_a$  is the dimensionless air-rivulet friction coefficient, which takes into account the friction effect of the wind on the rivulet;  $f_c$  is the (dimensional) rivulet-cable friction coefficient, which takes into account for the rivulet movement damping due to the energy dissipation between the rivulet and the cable (or, better, between the rivulet and the base carpet - see Part I).

The exciting aerodynamic forces are produced (Part I) by the interaction between the rivulet and the air boundary layer. For  $Re$  values close to the critical range (if the water roughness effect is taken into account - Part I) such interaction determines the reattachment of the separated boundary layer before the definitive separation (“one bubble regime”). The reattachment produces two effects: a local effect on the pressure field and the subsequent pressure gradients (thus, on the rivulet equilibrium) and a global effect on the cross-wind force. This regime occurs preferably during the descending (windward) rivulet movement, corresponding to a bigger and better marked rivulet (with respect to the ascending-leeward movement). Due to the synchronization between the rivulet and the cable movement, the downward lift force produced by the boundary layer reattachment is approximately in-phase with the cable velocity. Thus, a positive aerodynamic work is produced on the cable and, if the phenomenon is sufficiently strong and regular, the cable is excited.

It is important to observe that the “bubble regimes” (and, in particular, the “one bubble” one)

occur only on not too yawed - with respect to the incident wind direction - cables. In fact, such a regime disappears for yawed cylinders if the effective yaw angle  $\beta^*$  is larger than  $30^\circ \div 40^\circ$ , as reported by Bursnall and Loftin (1951).

Even if the phenomenon is stochastic, it is here treated in a deterministic way by taking into account the only “mean-cycle” effects (Part I). This is sufficient to represent the mean aerodynamic power acting on the cable. Hence, it is possible to define a function  $\Phi$  ( $0 \leq \Phi \leq 1$ ) to take into account the occurrence probability of the one “bubble regime”. Such a function is reasonably (see the above observations) dependent on the rivulet position and velocity, the Reynolds number (referred to the normal to the cable wind speed  $Re_n = U_0 \cos \beta^* / \nu$ ) and the effective yaw angle. Thus,

$$\Phi = \Phi(\varphi_R, \dot{x}, \beta^*, Re_n) \quad (4)$$

Once the occurrence function has been defined, the local (pressure modifications) and global (lift force) effects of the reattachment have to be evaluated. The effect on the pressure distribution can be considered by mean of a corrected pressure coefficient

$$Cp(\varphi, \Phi) = Cp_{und}(\varphi) + \Phi \cdot \Delta Cp(\varphi) \quad (5)$$

$Cp_{und}(\varphi)$  being the undisturbed pressure coefficient and  $\Delta Cp(\varphi)$  the one “bubble regime” induced local disturbance, as defined below. The effect on the global lift force can be taken into account by mean of a force, perpendicular to the instantaneous wind incidence,

$$F_{ex} = \frac{1}{2} \rho_a U^2 D \cdot C_{L,max} \cdot \Phi \quad (6)$$

$C_{L,max}$  being the global cross-wind force coefficient, corresponding to  $\Phi = 1$ .

### 3. Parameter calibration

The calibration of mechanical and aerodynamic parameters is based on both literature and experimental (Part I) data. Whenever reliable expressions are not provided by literature, the functional liaisons are determined and calibrated by fitting experimental results. Multiple-variable functions have been decomposed by mean of the variable-separation hypothesis.

#### 3.1. Cable drag coefficient

Experiments have pointed out that, in exciting conditions, the drag coefficient, referred to the mean wind speed normal to the cable, ranges from  $C_D=0.7$  to 1.3. In the present model an averaged value  $C_D=1.0$ , corresponding to the most frequent flow regime, is assumed.

#### 3.2. Rivulet dimensions

In Part I, it was observed that the rivulet dimensions varies along the cable “mean cycle”. The present model neglects such a variation in the rivulet equilibrium equation; the mean values are

assumed to be constant. Thus, the model considers the rivulet thickness  $t=0.15$  mm and its width  $l=6$  mm.

### 3.3. "Undisturbed" pressure distribution

The distribution law reported by Thompson (1980) is assumed for undisturbed (by rivulet) pressures around the cylinder. The pressure coefficient analytical expression is (Fig. 3):

$$C_{p_{und}}(\varphi) = 1 - (1 - C_{p_m}) \cdot \sin^2\left(90^\circ \frac{\varphi}{\varphi_m}\right) \quad \text{for } 0 \leq \varphi \leq \varphi_m \quad (7a)$$

$$C_{p_{und}}(\varphi) = C_{p_b} - (C_{p_b} - C_{p_m}) \cdot \cos^2\left(90^\circ \frac{\varphi - \varphi_m}{\varphi_b - \varphi_m}\right) \quad \text{for } \varphi_m \leq \varphi \leq \varphi_b \quad (7b)$$

$$C_{p_{und}}(\varphi) = C_{p_b} \quad \text{for } \varphi_b \leq \varphi \leq 180^\circ \quad (7c)$$

The parameters of Eq. (7) were calibrated by fitting the wind tunnel tests. In particular, for the wet yawed ( $\alpha=23^\circ$ ,  $\beta=30^\circ$ ) but not excited cable, they were found to be:

$$C_{p_b}=-1.5; \quad C_{p_m}=-3.2; \quad \varphi_b=118^\circ; \quad \varphi_m=85^\circ$$

These parameters are assumed to be constant even for different yaw angle. More suitable calibrations can be carried out by means of more wind tunnel tests for different yawing conditions and/or different Reynolds numbers.

### 3.4. Pressure distribution "disturbance"

The effect of air-rivulet interaction on the local pressure distribution has been analysed by evaluating the maximum difference between the pressure distribution in undisturbed conditions (no

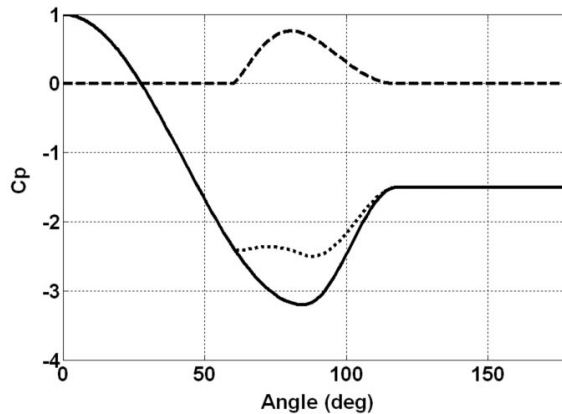


Fig. 3 Pressure distributions: solid=undisturbed; dashed=disturb ( $\Delta C_p$ ); dotted=maximally disturbed ( $\Phi=1$ )

rivulet) and in disturbed ones (rivulet-excited conditions) within the upper part of the cable, where the rivulet takes place and oscillates. The best fit of experimental data has been obtained by the following lognormal function:

$$\Delta C_p(\varphi) = 0.2 \cdot \exp \left[ -\frac{\ln^2 \left( \frac{\varphi}{80^\circ} \right)}{0.06} \right] \quad (8)$$

which is valid within the upper part of the cable, all over the rivulet oscillation region. The value of  $\Delta C_p(\varphi)$  given by Eq. (8) is used in Eq. (5). As a matter of fact, both the shape and the amplitude of the pressure disturbance probably depend on the rivulet position, that is  $\Delta C_p = \Delta C_p(\varphi, \varphi_R)$ . Nevertheless, the available experimental data were not sufficient to adequately calibrate such a two-variables relationship. In fact, the measured pressure distribution didn't show a clear correlation between the rivulet position and the location of the induced disturb. Hence, it has been assumed  $\Delta C_p = \Delta C_p(\varphi)$  and the  $\varphi_R$  influence has been limited to the disturbance amplitude by mean of the weight function  $\Phi$  which multiplies  $\Delta C_p$  in Eq. (5). Fig. 3 shows a plot of Eqs. (7), Eq. (8) and Eq. (5), the latter by assuming  $\Phi = 1$ , to show the maximally disturbed (by rivulet) pressure distribution.

### 3.5. "Disturbed" lift coefficient

The same principle as described in the previous section was followed to evaluate the global cross-wind (lift) force on the cable produced by the air-rivulet interaction. The maximum aeroelastic effect has been found to be  $C_{L, \max} \cong 0.8$ , referred to the mean wind speed normal to the cable. This value is used in Eq. (6).

### 3.6. Rivulet shape factor

The analysis of rivulet mean shape suggests a value  $\psi_v = 0.6$  which is adopted in the present model (it can be observed that  $\psi_v = 0.5$  for a triangle shape and  $\psi_v = 0.67$  for a parabola shape).

### 3.7. Skin friction

Zdravkovich (1997) reports that the skin friction coefficient  $f_a$  distribution around the cylinder, at sub-critical or close to critical  $Re$  values, is very close to the distribution of the pressure gradient (at least before the separation point, that is, within the region interested by the rivulet oscillations). Actually, such a similitude is not casual. In fact, the skin friction is proportional to the boundary layer velocity gradient which, in turn, is proportional to the pressure gradient. Of course, this liaison ceases to be true when the boundary layer separates (leeward the separation point) and/or it becomes turbulent (as for super-critical  $Re$ ). Nevertheless, within the region interested by the rivulet and for the  $Re$  range where RWIVs occur, the friction coefficient distribution around the cylinder can be assumed to be proportional to the pressure gradient, that is:

$$f_a(\varphi_R) = \frac{[f_a(\varphi)]_{\max}}{[\partial C_p(\varphi) / \partial \varphi]_{\max}} \left. \frac{\partial C_p(\varphi)}{\partial \varphi} \right|_{\varphi = \varphi_R} \quad (9)$$

where the proportionality coefficient  $[f_a(\varphi)]_{\max}$  can be evaluated by solving the rivulet equilibrium (Eq. (3)) in static conditions (by considering the minimum wind speed which allows the rivulet formation and the corresponding measured rivulet position). This evaluation has been made for different experimental tests. A reliable mean value is  $[f_a(\varphi)]_{\max} = 20 \cdot 10^{-3}$ , corresponding to  $[\partial Cp(\varphi)/\partial \varphi]_{\max} \cong -4.3$ ,  $\alpha=23^\circ$ ,  $\beta=30^\circ$ ,  $\theta \cong 40^\circ$ ,  $R=0.08$  m,  $U_{\min} \cong 6$  m/s,  $t=0.15$  mm.

For super-critical  $Re$ , the skin friction is characterised by a different law; not negligible skin friction appears leeward the separation point and it is responsible of the rivulet expulsion observed at high wind speed. As a matter of fact, such a regime is not interesting for RWIV study. In fact, during wind tunnel tests, it was observed that the RWIV stops at lower wind speed, before the rivulet is swept away. Thus, the “super-critical term” of skin friction is neglected in the present model.

### 3.8. Internal water damping

It is difficult to determine the damping (energy dissipation) between the rivulet and the base carpet over which it slides. A rough approximation can be made by assuming that such a damping is due to the water viscosity and by hypothesising a constant velocity gradient within the rivulet thickness (maximum velocity at the air-rivulet boundary and null velocity at the rivulet-base carpet boundary). Thus,

$$f_c \dot{x} = \mu_w \left. \frac{\partial \dot{v}}{\partial \eta} \right|_{\eta=0} \quad (10)$$

where  $\mu_w \cong 10^{-3}$  [N sec/m<sup>2</sup>] is water viscosity coefficient (Peube and Sadat 1993). If the rivulet shape is such that its geometrical centre is at approximately  $t/3$  from the base carpet boundary, it results

$$\left. \frac{\partial \dot{v}}{\partial \eta} \right|_{\eta=0} \cong \frac{\dot{x}}{t/3} \quad (11)$$

and thus

$$f_c \cong \frac{\mu_w}{t/3} \cong 30 \left[ \frac{N \cdot s}{m^3} \right] \quad (12)$$

which is the value adopted in the present model. It is important to observe that the above internal “friction” coefficient is strongly sensitive to the rivulet thickness and, hence, to the rainfall. This circumstance is confirmed by experimental data. In fact, low rainfalls give rise to very regular rivulet motion (thin rivulet, highly damped) while strong rainfalls give rise to irregular rivulet motion (thick rivulet, less damped and so sensitive to any turbulence and random fluctuation).

### 3.9. The “occurrence function”

Based on above reported observations, the “occurrence function”  $\Phi$  has been assumed to depend on the rivulet position, its velocity, effective yaw angle and Reynolds number. The multi-variable function has been decomposed as multiplication of four single-variable functions. Each of such functions has been assumed to be normal-derived type (when the depending variable is observed or

reasonably supposed to assume non-null values over a limited range of the independent variable) or arc-tangent type (when the depending variable is observed or reasonably supposed to vary between a lower threshold and upper one within a limited range of the independent variable). The parameters of each function have been calibrated by fitting (least squares method) experimental results (Part I) or literature data. Finally, the following expression has been found and adopted in the proposed model:

$$\Phi = \exp\left[-\left(\frac{\varphi_R - 90^\circ}{10^\circ}\right)^2\right] \cdot \left[0.5 + 0.45 \cdot \operatorname{arctg}\left(\frac{\dot{x}}{2 \cdot 10^{-3} \text{ m/s}}\right)\right] \cdot \exp\left[-\left(\frac{\beta^*}{40^\circ}\right)^4\right] \cdot \exp\left[-\frac{\ln^2(Re_n/10^5)}{0.2}\right] \quad (13)$$

Some comments to the above expression are opportune. The rivulet position dependent contribution shows a very narrow band centred around  $90^\circ$ ; in fact, the “one bubble regime” occurs only if the obstacle (rivulet) is close to the boundary layer separation point. The rivulet velocity dependent term is very close to a step function; in fact, as it was observed in Part I, the rivulet is well formed during its descending phase and it spreads during the ascending motion, drastically reducing the “obstacle effect”. Concerning the yaw angle dependent term, the data reported by Bursnall and Loftin (1951) about the occurrence of “bubbles regime” have been fitted. Finally, the  $Re$  dependent term has been fitted to the full scale observation data, as reported in literature since Matsumoto, *et al.* (1989). As a matter of fact, the experiments carried out in the climatic wind tunnel didn’t allow to monitor this term, because the cable model diameter was fixed (160 mm) and, thus, the  $Re$  dependence was just a wind speed dependence. Furthermore, even the full scale observations can be partially affected by this problem, the actual bridge stay cable diameters covering a not very wide range ( $D_{\max}/D_{\min} \approx 4$  as order of magnitude). Nevertheless, if the “one bubble regime” based interpretation of RWIVs is stated, the  $Re$  dependent term must be present in Eq. (13); of course, further specific wind tunnel tests are necessary to accurately calibrate this term.

It seems necessary to underline that, due to the complexity of the above reported functional liaisons, the estimated parameters are reliable only as order of magnitude. Nevertheless, it can be noted that all the used terms are significant in the dynamic equilibrium equations and, thus, in determining the excitation. This implies that too simplified models cannot completely describe the complex RWIV phenomenon.

#### 4. Numerical results and discussion

Eqs. (2) and (3) can be jointly solved by means of conventional iterative methods. In the present work, the procedure reported by Ben Kahla (1995) has been adopted. Different external conditions (wind speed, yaw angle, etc.) have been numerically tested and some significant results are going to be reported and discussed below.

Most of numerical investigation were referred to a cable model whose characteristics are close to the model tested in the CSTB wind tunnel as described in Part I. Unless differently indicated, the following properties have been assumed: cable diameter  $D=0.16$  m, cable mass per unit length  $m=20$  kg/m; in-plane cable frequency  $f_y=1.00$  Hz, out-of-plane cable frequency  $f_z=1.01$  Hz (the reason of such a small difference will be clarified below), damping ratio for both in-plane and out-of-plane modes  $\xi_x=\xi_y=0.1\%$ , cable inclination to the horizontal  $\alpha=23^\circ$ .

4.1. Cable displacements

Fig. 4 shows a typical time history trace of cable displacement during the excitation phase. The oscillation growth is quite linear until to reach the maximum amplitude. Some deviations from linear growth can occur due to adjustments in cable-rivulet synchronisation. This behaviour agrees with the wind tunnel results.

It was observed that the exciting force is approximately perpendicular to the wind incidence. Thus, the cable oscillation is expected to occur approximately perpendicular to the direction  $\gamma$ , as determined by Eq. (1). For instance,  $\alpha=25^\circ$  and  $\beta=30^\circ$  give  $\gamma=13^\circ$ , which is the expected trajectory

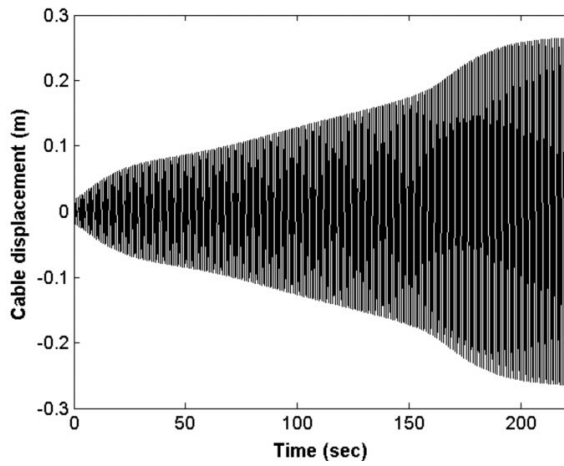


Fig. 4 Typical numerical response during the excitation phase:  $U=10$  m/s,  $\beta=20^\circ$

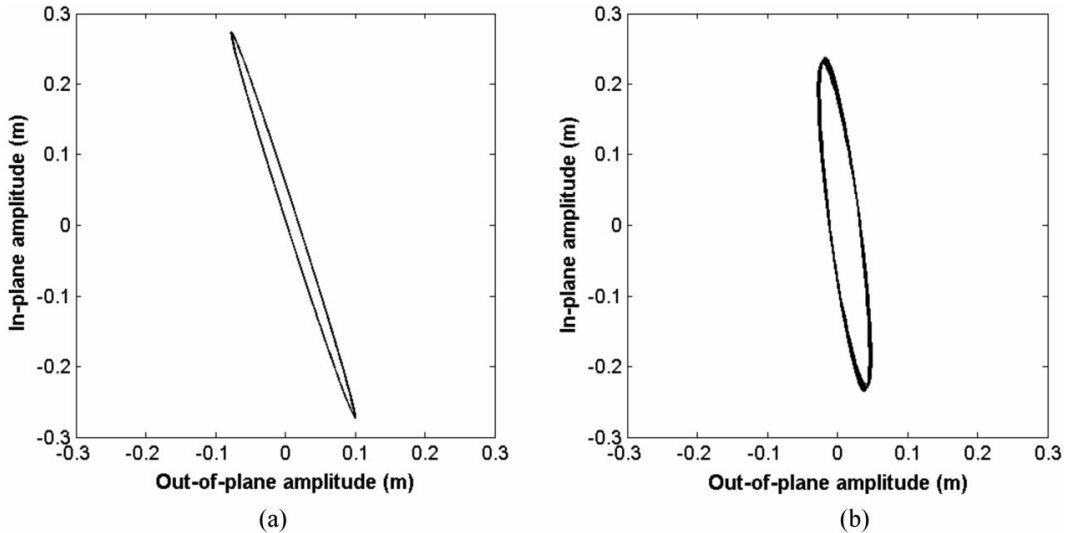


Fig. 5 Displacement locus from steady-state time histories: (a)  $U=10.5$  m/s,  $\beta=30^\circ$ ,  $f_x=f_y=1$  Hz and (b)  $U=10.5$  m/s,  $\beta=30^\circ$ ,  $f_x=1.01$  Hz,  $f_y=1$  Hz

inclination corresponding to those parameters. As a matter of fact, this is true only if both the in-plane and the out-of-plane motion are characterised by the same modal shape and modal frequency (Fig. 5(a)). In fact, even a very small difference between the two frequencies produces a trajectory rotation toward the in-plane direction (Fig. 5(b)). This explains the full scale observations, which mostly report movements close to the in-plane even when the cable is yawed to the wind. Furthermore, the cable trajectory can be influenced by the drag coefficient variations, during a “mean cycle”, which have not been considered in the present model.

#### 4.2. Wind speed and direction

The influence of the wind speed and its direction have been extensively analysed by varying  $U$  and  $\beta$  within the exciting range. Fig. 6 shows the results of such investigation relatively to above described cable model. Theoretical results are in very good agreement with the full scale observation features as reported in literature and summarised in Part I. In addition, it can be observed that, as the yaw angle increases, the exciting absolute wind speed range increases too. In fact, the rivulet dynamic equilibrium is strictly related to the wind speed component normal to the cable axis, which diminishes as the yaw angle increases.

The analysis of the rivulet equilibrium, Eq. (3), points out the reason why the wind speed and the yaw angle influence the RWIV mechanism. Different aspects are involved by the wind speed level. Firstly, the wind speed influences the Reynolds number and so the possibility of occurrence of the alternate flow regimes. Also, the rivulet equilibrium and its motion are influenced by the wind speed. In particular, up to a suitable wind speed (depending on the yaw angle) the water droplets fall down under the gravity effects and the upper rivulet cannot be formed. As the wind velocity increases, the pressure gradients and air-water friction forces are able to win the gravity and the upper rivulet is formed and oscillates. Because the aerodynamic exciting force is proportional to  $U^2$  and the aerodynamic damping is proportional to  $U$ , the excitation increases with the wind speed. On the other hand, as the wind speed further increases, the rivulet is “stiffened” by the increased

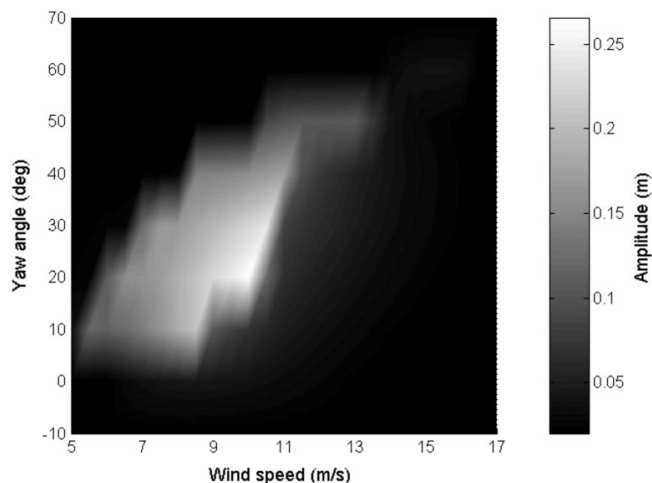


Fig. 6 In-plane oscillation amplitude for different wind speed and yaw angles, from numerical simulation:  $f_x=1.01$  Hz,  $f_y=1$  Hz

aerodynamic forces. Its movement, dimension variations and the subsequent excitation mechanism are reduced. Furthermore, for higher wind speed, the critical Reynolds number is approached; a friction force appears in the adverse pressure gradient region, as cited above, and the rivulet is swept away. Hence, there is a value of wind speed at which the excitation reaches its maximum before decreasing.

Concerning the yaw angle, the excitation occurs on cables declining to the wind direction which are lightly yawed. The RWIVs have been observed within the yaw angle range  $\beta=0^\circ$  to  $60^\circ$ , being  $\beta=20^\circ\div 30^\circ$  the worst conditions. These correspond to the yaw angle values which simultaneously allow: (a) the formation of a statically stable upper rivulet, (b) its excitability by cable acceleration effects, (c) the existence of the “bubble regimes”.

### 4.3. Cable frequency

Full scale observations (Main, *et al.* 2001) have widely reported that the RWIVs occur within a limited range of cable frequencies. In particular, the actually excited modes are characterised by a frequency included within the range 0.6 to 3.5 Hz. A wide frequency range has been numerically investigated by varying the cable stiffness (corresponding to a variable tension) and the mechanical damping coefficient (the damping ratio being kept to  $\xi=0.1\%$ ). The results are plotted in Fig. 7 and are in good agreement with the full scale observations (Main, *et al.* 2001).

An explanation of the cable frequency influence can be given by the proposed mechanical model. In fact, the exciting mechanism is based on the capability of the inertial effects (produced by the cable movement) to induce the rivulet oscillation and on the synchronisation of rivulet and cable movements without large phase lag. If the cable frequency is too low, the inertial effects are too small (at least at the beginning of the excitation) and are not able to excite the rivulet. Thus the incipient excitation is prevented. As the cable frequency increases, even small cable oscillations (for instance, produced by buffeting or deck motion) can induce significant inertial effects, the acceleration increasing with the frequency square. The rivulet begins to oscillate and the process becomes self-excited. On the other hand, if the cable frequency increases over the resonance threshold, the rivulet moves in counter-phase to the cable and the excited process is inverted. The rivulet effect is to damp the cable motion.

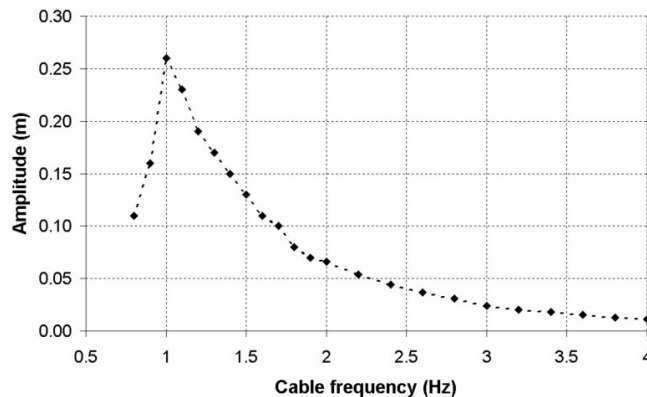


Fig. 7 Cable oscillation amplitude vs cable frequency:  $U=10$  m/s,  $\beta=20^\circ$ ,  $f_x=1.01 f$ ,  $\xi=0.1\%$

Even if a 3D model is necessary to predict the cable mode excited by RWIVs, it seems reasonable to suppose that the mode whose frequency is closer to the more sensitive one (depending on the cable diameter,  $\alpha$  and  $\beta$ ), can be the excited one.

#### 4.4. Cable diameter

All the existing cables which have been excited by the rain-wind combined action are characterised by a diameter within the range 80 to 250 mm. This circumstance can be explained by keeping in mind two already cited features: (a) the Reynolds number is approximately within the range  $Re=80000$  to  $150000$  to allow the reattachment of the separated flow; (b) the wind speed has to be high enough ( $\sim >8$  m/s) to allow the rivulet equilibrium but not so much ( $\sim <16$  m/s) to avoid the rivulet stiffening or expulsion. Thus, the cable diameter range compatible with both the above conditions is approximately  $D=80$  to  $250$  mm.

#### 4.5. Cable surface

The cable surface wet-ability plays an essential role as pointed out by Flamand (1995). As a matter of fact, the wet-ability allows the formation of the water “base carpet” over which the rivulet slides. On the contrary, a water repellent surface doesn’t allow the cable to be covered by a water carpet and the mobile rivulet has to slide directly on cable encasing. The surface tension becomes not negligible and it can stiffen the rivulet. Furthermore, the asymmetric rivulet motion described in Part I and mostly responsible of the excitation, is strongly opposed by the surface tension.

As a matter of fact, the surface wet-ability allow also the formation of a water carpet all over the cable circumference which modifies the cable roughness and, subsequently, the air flow regime. Of course, this effect has to be further investigated and clarified. Anyway, wind tunnel tests have to carefully reproduce it. Hence, the experiments carried out in dry conditions by artificial solid rivulets probably neglect important aspects.

#### 4.6. Influence of rainfall and wind turbulence

A regular rivulet motion (synchronised to the cable one) allows the occurrence function, which actually is a stochastic function, to be less “random” and, thus, to better “follow” the cable movement. Subsequently, the exciting mechanism is helped by a regular rivulet oscillation. This explains why the major RWIVs have been observed under moderate rainfalls and low turbulent winds. In fact, both the rainfall and the incident wind turbulence influence the regularity of the rivulet oscillation (the former acting on the rivulet thickness and, hence, on the damping of the associated oscillator -see Eq. (12) - which, in turn, influences the motion regularity). Furthermore, a certain correlation between rainfall and wind turbulence has been hypothesised by some scientists.

## 5. Conclusions

Following a wide experimental investigation and the physical interpretation of rain-wind induced vibration (RWIV), as given in Part I, a mechanical model of the exciting mechanism has been proposed in this paper. It is a simplified model (cross-sectional and deterministic) of the actual stochastic and three-dimensional phenomenon. Hence, the longitudinal correlation effects are not

taken into account and the excited natural mode has to be selected a priori, as a model input.

The model is based on measurements performed on a 160 mm cable model. It seems reliable, as the real cables used in bridge engineering rarely exceed this dimension more than 50%, but it should be valuable to realize further experiments of the same kind on bigger and smaller cables.

A wide range of external conditions (wind and cable characteristics) has been numerically investigated. The results show that the proposed model is able to keep all the main features of full scale observations. For instance, the sensitivities to the cable diameter and frequency, the limited wind speed range and the oscillation direction are well reproduced by numerical analysis.

Due to the complexity of the functional liaisons which characterise the dynamic equations, some estimated model parameters are reliable only as order of magnitude and further experiments, specifically oriented to an accurate calibration of such parameters, are required.

Nevertheless, since the proposed model well simulates the occurrence and the characteristics of cable RWIVs, it represents a good base for the formulation of a definitive predictive model to use in designing or retrofitting stay cables against RWIVs.

## References

- Ben Kahla, N. (1995), "Dynamics of single guy cable", *Computers and Structures*, **54**(6), 1197-1211.
- Bursnall, W.J. and Loftin, L.K. (1951), "Experimental investigation of the pressure distribution about a yawed circular cylinder in the critical reynolds number range", NACA TN 2463, Washington.
- Cosentino, N. (2002), "Rain-wind induced vibrations of stay cables", Ph.D. Thesis, University of Bologna, Bologna.
- Cosentino, N., Flamand, O. and Ceccoli, C. (2003), "Rain-wind induced vibration of inclined stay cables. Part I: experimental investigation and physical explanation", *Wind Structures, an Int. J.*, **6**(6), 471-484.
- Flamand, O. (1995), "Rain-wind induced vibration of cables", *J. Wind Eng. Ind. Aerodyn.*, **57**, 353-362.
- Geurst, C., Vrouwenvelder, T., Staalninen, P. and Reusink, J. (1998), "Numerical modelling of rain-wind-induced vibration: erasmus bridge, rotterdam", *Structural Engineering International*, **2**, 129-135.
- Main, J.A., Jones, N.P. and Yamaguchi, H. (2001), "Characterisation of rain-wind induced stay-cable vibrations from full-scale measurements", *Proceedings of 4th International Symposium on Cable Dynamics*, Montréal, May.
- Matsumoto, M. (2000), "Vortex-excited vibration and galloping instability of inclined cables", *Proceedings of 6th Italian Conference on Wind Engineering, IN-VENTO-2000*, Genova, June.
- Matsumoto, M., Yokohama, K., Miyata, T., Fujino, Y. and Yamaguchi, H. (1989), "Wind-induced cable vibration of cable-stayed bridges in Japan", *Proceedings of Japan Canada joint Workshop on Bridge Aerodynamic*, Japan.
- Peube, J.L. and Sadat, H. (1993), "Oscillations aeroelastiques des haubans de ponts a haubans sous les effets conjugués du vent et de la pluie", Rapport Université de Poitiers, Portiers.
- Ruscheweyh, H.P. (1999), "The mechanism of rain-wind-induced vibration", *Proceedings of Wind Engineering into the 21st Century*, Rotterdam.
- Thompson, N. (1980), "Mean forces, pressures and flow field velocities for circular cylindrical structures: single cylinder with two-dimensional flow", ESDU Data Item 80025, London.
- Verwiebe, C. and Ruscheweyh, H. (1998), "Recent research results concerning the exciting mechanisms of rain-wind-induced vibration", *J. Wind Eng. Ind. Aerodyn.*, **74-76**, 1005-1013.
- Yamaguchi, H. (1990), "Analytical study on growth mechanism of rain vibration of cables", *J. Wind Eng. Ind. Aerodyn.*, **33**, 73-80.
- Zasso, A., Bocciolone, M. and Brownjohn, J. (1992), "Rain-wind aeroelastic instability of the inclined hangers of a suspension bridge", *Proceedings of Inaugural Conference of the Wind Engineering Society*, Cambridge, September.
- Zdravkovich, M.M. (1997), *Flow around Circular Cylinders*, Oxford University Press, Oxford.